Water Practice & Technology

IWA PUBLISHING

Water Practice & Technology Vol 18 No 5, 1300 doi: 10.2166/wpt.2023.063

Modelling future flood events under climate change scenarios in the Pungwe River Basin

Moises de Jesus Paulo Mavaringana [a,b,*], Webster Gumindoga[b], Jean-Marie Kileshye Onema[c,d] and Hodson Makurira[b]

[a] Divisão de Agricultura, Instituto Superior Politécnico de Manica, P.O. Box 417, Manica, Mozambique
[b] Construction and Civil Eng. Department, Box MP 167 Mt Pleasant, University of Zimbabwe, Harare, Zimbabwe
[c] Waternet, P.O. Box MP600, Mount Pleasant, Harare, Zimbabwe
[d] School of Engineers, University of Lubumbashi, Lubumbashi, DR Congo
*Corresponding author. E-mail: jesusmavaras@gmail.com; moises.mavaringana@students.uz.ac.zw

M de JP, 0000-0003-2986-8674

ABSTRACT

This study sought to project future changes in hydroclimatic variables and to establish how climate change affects flood inundation extent in the Pungwe River Basin. Climate ensembles of 10 Regional Climate Models from the CORDEX project were selected. The historical rainfall and temperature time series and the downscaled climate data were input into the HBV model to generate streamflow for the 2022–2099 period. Flood extents for 50-, 100-and 1,000-year return periods were predicted using the HEC-RAS hydraulic model. By 2070, annual rainfall at all nine studied meteorological stations is predicted to reduce by a maximum of 61%. Temperature is expected to increase up to 1.5% over the same period. By the 2070s, simulations from HBV revealed that the peak flows for the Pungwe River Basin will increase by up to 100% and decrease by approximately 57% as projected by the model ensemble. The analyses also show that by 2070 climate change may cause a minimum of 2,784.4 km^2 and a maximum of 8,235.6 km^2 of flood extension. These results are essential for decision-making on flood hazard mapping and early warning systems, prompting a pathway for sustainable development.

Key words: inundation extent, regional circulation models, return period, streamflow simulation, flood mapping

HIGHLIGHTS

- Satellite rainfall estimates, RCMs, hydrological, and hydraulic models for flood inundation extent mapping.
- By 2070, the future projections show increasing temperature and decreasing rainfall.
- Climate change will, however, increase peak flows and inundation extent by the 2070s.
- Significantly affected places in the Pungwe River Basin include cropland, built-up areas, roads, schools, hospitals, and business infrastructure.

GRAPHICAL ABSTRACT

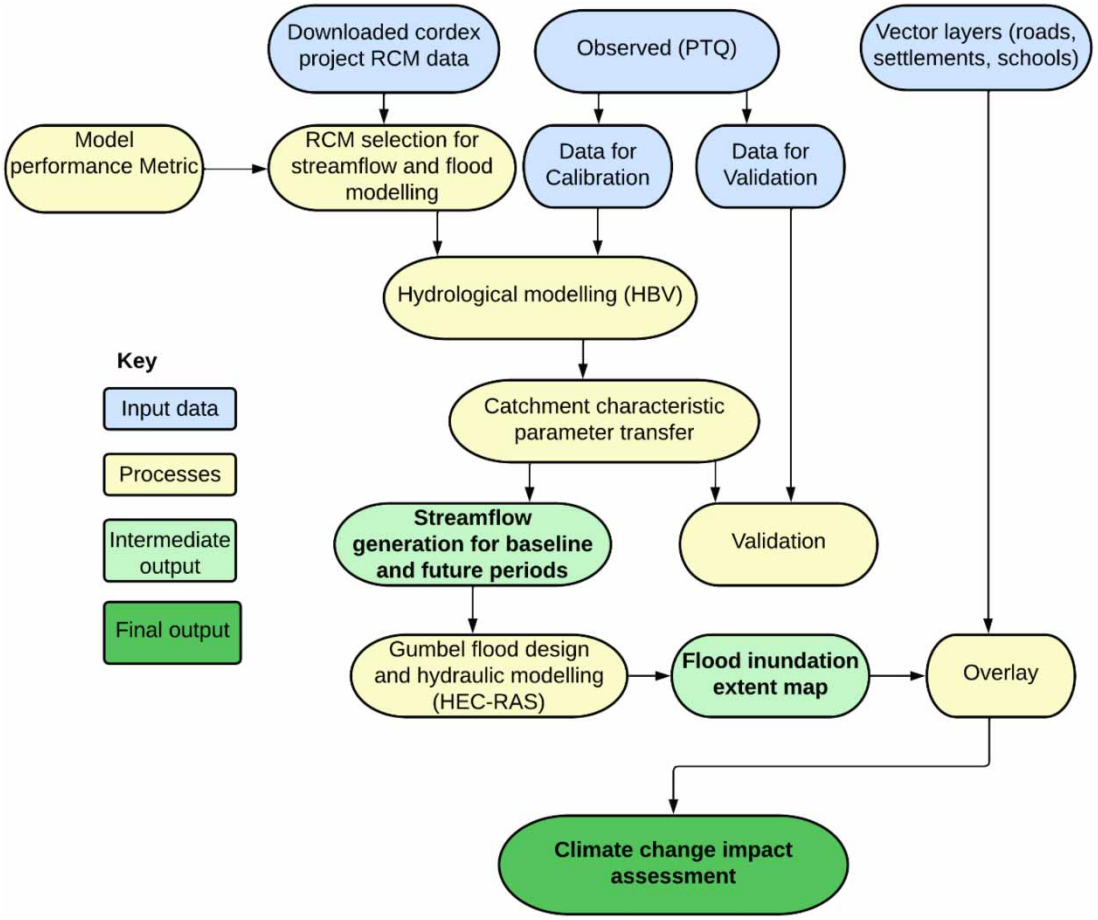

INTRODUCTION

Climate change has direct impacts on ecosystems and the services they provide to society, thus influencing human well-being, health (Kalantari *et al.* 2018), and increasing water-related extremes such as floods events, with significant impacts on the economy and environment (Di Baldassarre *et al.* 2017). Flood occurs due to rapid population growth, land degradation, and climate change (Desalegn & Mulu 2021). To reduce the effects of water-related natural hazards and their societal effects, it is imperative to create more efficient strategies, methods, and tools for incorporating water-based analyses, such as flood mapping into spatial planning, especially in the most vulnerable countries (Kalantari *et al.* 2018; Korah & Cobbinah 2019);

The latest IPCC report claimed that extreme environmental conditions, including extreme floods, will become unprecedented in magnitude, frequency, and timing in high-risk areas and new regions not typically prone to natural disasters (IPCC 2021). This report claim call for hydrological research and assessment of climate change impacts as a central issue at all levels (Korah & Cobbinah 2019). In fact, several climate change impact studies have been done, but the gap is that they characterize African River Basins and cities therein as homogenous, experiencing the same climate events and requiring the same planning solutions (Gaisie & Brandful 2023). However, African River Basins and cities are diverse and different across regions, scales, and contexts, despite some resemblance of their settlement's problems (Ramayanti *et al.* 2022; Gaisie & Brandful 2023). The Pungwe River Basin is vulnerable to the adverse effects of climate change such as flooding on a yearly basis due to its downstream characteristic, coastal proximity, and exposure (Williamson *et al.* 2023), representing a high risk of damage to the community, infrastructure, destruction of livestock and loss of life. For example, tropical Cyclone Idai struck the coastal city of Beira, on 14 March 2019. The cyclone brought heavy rain accompanied by strong winds that lasted for more than a week (Government of Mozambique 2019; Ramayanti *et al.* 2022). As a result, the Pungwe and Buzi Rivers Basins overflowed and inundated low-lying

areas (Guo *et al.* 2021). This disaster caused 4,000 houses to be damaged or inhabitable, about 1,600 people were injured, and 603 people were killed in Mozambique, Zimbabwe, and Malawi (UNDP 2019).

Therefore, flood hazard maps are an essential tool to help planners and decision-makers to better understand the spatial distribution of hypothetical flood characteristics more directly and easily (Grežo *et al.* 2020; Chen *et al.* 2022) and provide necessary information for many strategies for mitigating, managing flood and setting policies for land development and insurance (Liu *et al.* 2021). Scientifically, two main approaches can be used for flood mapping and risk assessment (Chen *et al.* 2022). The first one involves using indicators to assess flood risk with the application of geographic information systems (GIS) and multi-criteria analysis (MCA) to estimate current and future flood risk maps (Rahmati *et al.* 2016; Chakraborty & Mukhopadhyay 2019). This approach is limited by the need for exploiting experts' knowledge in assigning weights, which can be considered a source of bias (Rahmati *et al.* 2016). The other approach simulates flood event variables, such as peak discharge and flood inundation, using hydraulic and hydrologic models under varied conditions. Hydrologic models such as HEC-HMS (Gumindoga *et al.* 2016; Nharo *et al.* 2019), and TOPMODEL (Januário *et al.* 2022) were used for streamflow simulation. Gumindoga *et al.* (2016) applied HEC-HMS for ungauged runoff simulation in the Upper Manyame Catchment of Zimbabwe. Different authors have also used hydraulic models such as HEC-RAS (Chipere *et al.* 2020) and SOBEK (Yue *et al.* 2022) for flood inundation mapping. Desalegn & Mulu (2021) used HEC-RAS for mapping flood inundation areas at Fetam River, Upper Abbay Basin, in Ethiopia. The study discovered that flooded areas in the upstream and middle parts of Fetam River are high as related to the downstream parts, which aided in mapping high-hazard areas.

That said, the serious impact of floods on the environment, the extensive damage to infrastructure, and human well-being in the cities located in and along the Pungwe River Basin is an important reason to assess flood mapping extent risk. Flood mapping identifies areas most vulnerable to flooding based on physical characteristics (Ramayanti *et al.* 2022). The maps of flood extent should be accurate and rapidly obtainable because it is essential for flood prevention and mitigation (Zare & Schumann 2021). However, the limited time available to map all areas, impractical fieldwork, or traditional hydrological methods is the challenge to generating an accurate map (Rahmati *et al.* 2016; Ramayanti *et al.* 2022). Therefore, since high-impact events such as floods often span spatial scales larger than those covered by traditional regional monitoring, integrating remotely sensed data with flood modelling, especially via satellite, is an appealing approach to the quick, fair, and accurate assessment of flood events, real-time monitoring and design of early warning systems (Schumann *et al.* 2018; Nharo *et al.* 2019).

This study advocates for using GIS, Earth observation, hydrological, and hydraulic modelling techniques with HBV and HEC-RAS to map the spatial extent of floods and assess the impacts of these floods in the context of climate change. To the author's knowledge, this is the first study to attempt the integration of all those models in generating flood extent maps. It is therefore significant to improve knowledge of mapping floodplains areas, and knowledge of catchment precipitation patterns in the basin in the face of climate change and variability to inform development pathways, and land and water management options (Nyabeze 2021). Specifically, the objectives of this study are: (i) to project future changes in climatic variables for the mid-2050 and 2080s; (ii) calibrate the HBV model and estimate future changes in extreme and seasonal streamflow due to climate change; (iii) estimate the flood inundation extent for various return periods (50, 100 and 1,000 years) in the context of future climate. The results of this study are important for the development of policies and strategies for flood management, map areas for urban and social infrastructure development, development of early warning systems, and technical assistance for water and not water-related specialists. The final products of maps for inundation extents herein presented can be used by institutions such as the Regional Water Administration – Centre of Mozambique (ARA-Centro), the National Disaster Management Institute (INGD), National Meteorological Institute (INAM).

METHODS

Study area selection and description

The Pungwe River Basin is located between the latitudes 18S and 20S and the longitudes 33E and 35E in the Sofala and Manica provinces, in the central part of Mozambique (Ramayanti *et al.* 2022). It has approximately 400 km in length and has a drainage area of 31,000 km^2, shared by Zimbabwe and Mozambique. 340 km of its length is located within Mozambique (Uamusse *et al.* 2015). The region of the Pungwe River Basin has a climate with a dry and a wet season. The dry season is between April and September, and the wet season is from

October to March. It stretches over two climate types; in the west is the humid mountainous climate of the high mountains that forms the border between Zimbabwe and Mozambique. In this region, the mean annual rainfall can reach above 2,000 mm, and the temperature is substantially lower than in the surrounding, non-mountainous areas (Uamusse *et al.* 2015). The western parts of the Basin consist of argillaceous red soils of a considerable depth. In mountainous areas, the soils are shallower but can reach more considerable depths in the valleys. The region's soils below the plateau are more varying and classified as clayey–sandy fluvial dark soils, fertile fluvial soils, or shallow soils without agricultural potential (SWECO and Associates 2004). The Pungwe River Basin was selected for this study for being prone to hydrometeorological hazards, associated with tropical cyclones such as flood events, every year due to its physical characteristic and proximity to the coastal areas (Ramayanti *et al.* 2022). Figure 1 shows the study area location.

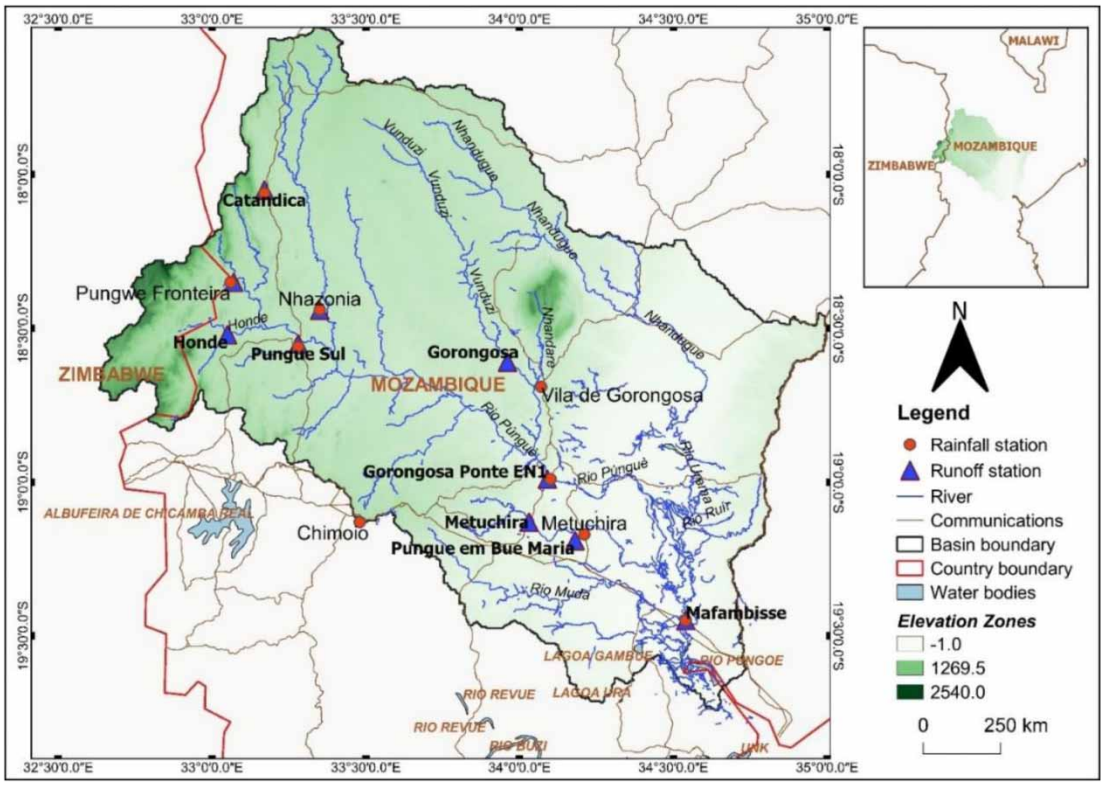

Figure 1 | Study area showing rivers, communications, elevations zones, rainfall, and runoff stations.

Source of data

Hydrometeorological data

Observed Hydrometeorological data were obtained from Administração Regional de Águas do Centro – ARA-Centro (Regional Water Administration – Centre) and Instituto Nacional de Meteorologia – INAM (Meteorology National Institute) of Mozambique, respectively. The data were from nine stations in the basin (Table 1).

The data consist of rainfall, maximum and minimum temperatures, and daily discharge (Gorongosa Ponte station). Due to the short length and breaks on the record of the time series of the observed data, *Satellite Rainfall Estimates* data were used to supplement the missing values within the observed data and for years where observed historical data were absent using data from NASA power data portal (https://power.larc.nasa.gov/data-access-viewer/). The satellite data were downloaded using coordinates for each station and consisted of 39 years (1981–2020). Before its use, the data were bias-corrected using a genetic algorithm for determining the Bias Factor (Habib *et al.* 2014). The Bias Factor was based on the Time–Space Variable (*TSV*), where the

Table 1 | Location, length of record, percentage of gaps on the data, and timestep record of rainfall and runoff stations

			Rainfall			Runoff		
Station name	**Long.**	**Lat.**	**Year of record**	**%Gaps**	**Timestep**	**Year of record**	**%Gaps**	**Timestep**
Vila de Gorongosa	34.07	−18.69	1991–2020	4	daily	–	–	–
Pungwe Sul	33.28	−18.56	1998–2020	6	daily	–	–	–
Nhazonia	33.35	−18.44	2001–2020	5.5	daily	–	–	–
Catandica	33.17	−18.06	1998–2020	3.7	daily	–	–	–
Metuchira	34.21	−19.17	1998–2020	10.2	daily	–	–	–
Gorongosa Ponte	34.10	−18.99	2009–2020	3.8	daily	1998–2015	6.8	daily
Mafambisse	34.54	−19.45	2017–2020	11.1	daily	–	–	–
Chimoio	33.48	−19.13	2012–2020	54.3	daily	–	–	–
Pungwe Fronteira	33.06	−18.35	2007–2016	6.2	monthly	–	–	–

bias is estimated for a particular location and a particular day. The procedure to determine the factor is stated in the following equation:

$$BF_{TSV} = \frac{\sum_{t=d}^{t=d-1} P_{sat}(i,t)}{\sum_{t=d}^{t=d-1} P_{obs}(i,t)} \quad (1)$$

where BF_{tsv} is the Bias Factor (BF) based on TSV; P_{sat} is the satellite rainfall estimates (mm); P_{obs} is the observed daily rainfall at the gauge (mm); i is the gauge location, t is the Julian day number (day), and l is the length of a time window for bias calculation.

Regional Climate Model data

Regional Climate Models (RCMs) used in this study were downloaded from the CORDEX-Africa (https://esg-dn1.nsc.liu.se/search/cordex/) runs downscaled from 10 GCMs of the Climate Model Inter-comparison Project Phase 5 (CMIP5) (Chipere *et al.* 2020). The latest version of the regional climate model by the Swedish Ross Centre's regional Atmospheric model – RCA4 was used for this study. It features an improved physical and energy flux parametrisation, and its modified radiation scheme has considered the absorption and concentration of carbon dioxide. Based on the recommendations of the land-use information, a quadrilled land surface scheme is proposed. The scheme consists of one to three key tiles, and the spatial resolution of the simulations for the CORDEX-Africa domain is 0.44 × 0.44. The projections are for 1951–2100 for both historical and future periods, 1951–2005 and 2006–2100, respectively. The projections were for RCPs 4.5 and 8.5 for two periods near the future (2022–2060) and far future (2061–2099). These models have been evaluated in multiple studies on Africa, and have been found to perform well in simulating rainfall and temperature (Worku *et al.* 2018; Dibaba *et al.* 2019). The RCA4 simulations used and evaluated in this study are described in Table 2.

Bounding uncertainty in RCMs and performance criteria

RCMs are used for forecasting future climate, including rainfall and temperature characteristics (IPCC 2014). Therefore, to effectively quantify the impacts of climate change at the local scale, it is necessary to select appropriate RCMs (Dibaba *et al.* 2019). Each model, however, exhibits some instances of bias therefore the use of a single RCM for climate change impact analysis gives room for further disputed uncertainty (Chipere *et al.* 2020). To reduce uncertainty, this study made use of the multi-model ensemble approach. As such, using the observed baseline daily data, the performance of the selected climate models in mimicking past observed temperature and rainfall was assessed using the performance metric utilised in several past studies (Dibaba *et al.* 2019; Demissie & Sime 2021) namely Nash–Sutcliffe Efficiency (*NSE*), Root Mean Square Error (*RMSE*), coefficient of determination (R^2), and index of agreement (d).

Table 2 | Selected RCMs for RCP4.5 and RCP8.5 scenarios

RCMs	Institution
CanESM2	Canadian Centre for Climate Modelling and Analysis
CNRM-CM5	Centre National de Recherches Meteorolo-Giques/Centre European de Recherche et Formation Avanceesencalcul scientifique of France
CSIRO-Mk3-6-0	Commonwealth Scientific and Industrial Research Organisation Mark 3.6.0
ESM2M	NOAA Geophysical Fluid Dynamics Laboratory
EC-EARTH	Irish Centre for High-End Computing
CM5A-MR	Institut Pierre Simon Laplace
MIROC5	Model for Interdisciplinary Research on Climate
HadGEM2-ES	Met Office Hadley Centre
MPI-ESM-LR	Max Planck Institute ESM, low resolution
NorESM1-M	Norwegian ESM, version 1, intermediate resolution

Projected changes in future hydrometeorological variables

Projected percentage change in the seasonal cycle climatology of temperature and rainfall relative to baseline mean (1982–2020) under RCP4.5 and RCP8.5 was computed by the following equation (Lawin *et al.* 2019).

$$P_n = \left(\frac{R_n - B_n}{B_n}\right) \times 100 \tag{2}$$

where P_n is the projected percentage change to the long-term historical mean for an nth month; R_n is the mean of projected temperature or rainfall for month n (long-term monthly mean); B_n is the mean obtained from the baseline years (long-term mean). The formula on Equation (2) represents the relative climatology, and it is going to be used to analyse the rainfall behaviour. For temperature analysis, absolute values of changes will be used as they represent better the changing of this variable in a great area such as the Pungwe River Basin. The systematic and dynamic behaviour of the models was also visualised by plotting the projections on the same coordinate system (Demissie & Sime 2021). For the purpose of analysing the projected changes, only four stations used by ARA-Centro for flood warning (SAC) were assessed, namely Nhazonia, Mafambisse, Pungwe Sul, and Gorongosa Ponte stations.

HBV model set-up

Computer models are frequently used for catchment hydrology studies. The HBV model (Bergström 1976) belongs to the conceptual class of hydrological models, characterised by attempts to cover the most essential runoff-generating processes using a simple and robust structure and a small number of parameters. The model consists of three main modules: snow accumulation and melt, soil moisture accounting, river routing, and response modules. This model is often used in discharge simulation, flood forecasting, and assessment of environmental change (Poméon *et al.* 2017; Hegdahl *et al.* 2023). The Shuttle Radar Topographic Mission 30-m resolution digital elevation model downloaded from https://earthexplorer.usgs.gov/ was used to delineate the watershed and extract terrain-specific characteristics. The DEM was used for DEM hydro-processing in the Integrated Land and Water Information System (ILWIS) to obtain hydrological features. Maathuis & Wang (2006) procedure for DEM hydro-processing has been used in the Pungwe River Basin for flow determination, drainage network and catchment extraction. From the process, eight sub-basins have been defined for further study analysis in the basin.

The Thiessen polygon method was used in this study to spatially estimate different meteorological variables over the Pungwe River sub-basins. This method gives the weight of each station data in proportion to the area covered in each sub-basin. However, apart from that, it clearly shows which station measurements are considered to have power in the basin whether the stations are located inside the latter or not (Brassel & Reif 1979). Calculating the ratio of each polygon area and the entire basin gives the weight of the station gauge at each sub-basin, there the spatial representation of the meteorological data over the entire basin or a sub-basin is calculated by the

following equation:

$$\overline{P} = \frac{1}{A}\sum_{i=1}^{n} A_i * P_i \tag{3}$$

A PTQ-file (ptq.txt) that contains time series of daily precipitation (mm/day), temperature (°C), and discharge (mm/day) was created. One PTQ-file was created containing all the sub-basins. Using ILWIS GIS, the slicing algorithm was applied to the Pungwe River Basin raster map to create the elevation zones. From the filled DEM, the elevation ranged from 206.13 to 1,649.04 m. From the DEM, eight classes were divided at a minimum elevation interval. Three vegetation zones in HBV were selected. Land-use images were acquired from CCI land cover – S2 prototype land cover 20 m map of Africa 2016 with a spatial resolution of 20 m × 20 m and imported to ILWIS. Initially, the image had more than three vegetation zones reduced to three using an 'IFF' function. The vegetation and the elevation zones maps were crossed, and the product was crossed again with the sub-basins map. For each sub-basin 24 elevation, vegetation zones were created. Before crossing, the maps were resampled to ensure they were in the same geo-reference system.

HBV model calibration and validation

The calibration is the estimation of the parameters that enable the model to match the real system's behaviour (Van Tiel *et al.* 2020). In this study, manual calibration was carried out by searching the parameter values that maximise the model's reliability (Hegdahl *et al.* 2023). The calibration period was from 2000 to 2010. Before calibration, 1999–2000 was used for model warmup. The validation period was from 2011 to 2015. The calibration and validation were done using the dataset for catchment 1, on which the data series had consistency and reliability for modelling and analysis. The calibrated and well-optimised model parameters were kept constant to generate streamflow for the baseline and future periods. To analyse the performance of the simulation, the *NSE*, coefficient of determination (r^2), mean difference (*MD*), efficiency on peak flow (*EPF*), and standard deviation (σ) were used.

Flood design and inundation simulations in HEC-RAS

The Hydrologic Engineer Center's River System Analysis System (HEC-RAS) software version 6 and the QGIS were used for hydraulic simulations and flood inundation mapping (Brunner 2008). The Pungwe River Basin 30 m SRTM DEM downloaded from https://earthexplorer.usgs.gov/ was used to create Geometric layers such as the stream centerline, bank lines, flow path centerlines and cross-section for the Pungwe, Nhazonia, Urema, Metuchira, Nhacarangue, Mucombezi, Messambize, Nhancangale, Vunduzi, and Nhadungue rives were created from the DEM. Manning's coefficients were defined as 0.02 for the channel and 0.03 for the riverbanks based on the field observation of the land-use practices. The discharge peaks for the near and far future at different timesteps derived from the HBV model and statistically predicted for 50-, 100- and 1,000-year return periods using Gumbel Extreme value were used for future flood inundation modelling under climate change scenarios. Inundation extents were computed for the historical and future periods. The flood extent was validated using the Cyclone Idai-induced flood on 19 March 2019.

RESULTS AND DISCUSSION

Projected changes in hydrometeorological variables

Performance metric of climate change models

To project changes in rainfall and temperature, first, the performance of RCMs were assessed and to unbound uncertainty associated with climate models, 10 models have been studied on simulating the rainfall and temperature of the Pungwe River Basin and a multi-model ensemble approach have been adopted for further analysis (Dibaba *et al.* 2019). This approach has been used by Chipere *et al.* (2020) to study future flood inundations under Climate Change in Middle Zambezi Basin in Zimbabwe. On the results of the study, the authors verified on the analysis of the historical GCM ensemble data against station data daily, that the GCM's ensembles were able to capture most of the peak precipitation periods for each catchment. This approach is crucial for the purposes of establishing flooding events in the past. Table 3 shows the results of the performance of the climate change models analysed at a daily timestep. The overall analysis shows that the models performed well on

Table 3 | Performance of RCMs on simulating hydroclimatic variables for the Pungwe River Basin analysed daily

		Goodness-of-fit				
Rank	**RCMs**	**Variables**	***NSE***	***RMSE***	***d***	r^2
1	CanESM2	Rainfall	0.68	9.4	0.88	0.56
		*T*max	0.78	3.9	0.68	0.77
		Tmin	0.76	2.74	0.86	0.81
2	CNRM-CM5	Rainfall	0.61	11.2	0.88	0.67
		*T*max	0.71	5.1	0.8	0.65
		Tmin	0.74	3.4	0.88	0.71
3	EC-EARTH	Rainfall	0.59	6.5	0.87	0.48
		*T*max	0.69	4.3	0.61	0.8
		Tmin	0.64	5.5	0.77	0.74
4	ESM2M	Rainfall	0.52	8.4	0.85	0.52
		*T*max	0.6	3.9	0.77	0.69
		Tmin	0.58	2.6	0.81	0.83
5	CSIRO-Mk3-6-0	Rainfall	0.51	13.9	0.86	0.5
		*T*max	0.51	4.4	0.68	0.66
		Tmin	0.6	2.5	0.74	0.59
6	CM5A-MR	Rainfall	0.51	10.7	0.82	0.59
		*T*max	0.6	4.1	0.69	0.77
		Tmin	0.56	3.1	0.78	0.71
7	MIROC5	Rainfall	0.50	8.5	0.84	0.45
		*T*max	0.55	3.9	0.67	0.8
		Tmin	0.44	5.2	0.75	0.8
8	HadGEM2-ES	Rainfall	0.48	8.8	0.77	0.51
		*T*max	0.5	3.5	0.59	0.54
		Tmin	0.67	2.4	0.77	0.46
9	MPI-ESM-LR	Rainfall	0.44	12.6	0.79	0.52
		*T*max	0.57	4.1	0.57	0.65
		Tmin	0.69	3.3	0.49	0.6
10	NorESM1-M	Rainfall	0.41	7.4	0.80	0.49
		*T*max	0.7	4.6	0.71	0.49
		Tmin	0.77	2.9	0.59	0.38
	Ensemble	Rainfall	0.71	6.1	0.88	0.75
		*T*max	0.78	2.7	0.92	0.77
		Tmin	0.86	3.4	0.94	0.85

temperature analysis compared to rainfall; this happened because rainfall has greater spatial and temporal than temperature (Masimba *et al.* 2019).

Projected change in long-term monthly mean rainfall

The projections of monthly long-term average rainfall under RCP4.5 and RCP8.5 scenarios show mixed signals, an increase and a decrease, compared to the baseline period, depending on the station (Figure 2). In the 2050 and 2080s, the multi-model ensemble shows similar behaviours in all the analysed SAC stations, an increase (up to 40%) and a decrease (up to 60%) for mid-range RCP4.5 and high-level RCP8.5 climate scenarios. However, in the future periods, Gorongosa Ponte station rainfall amounts will decrease for the month of October (60%) November (35%) and December (37%) under RCP4.5 during the 2050s. For the second half of the summer season, rainfall amounts will increase for the month of January (10%), and decrease in February (39%) and March (57%) for the 2080s. For RCP8.5 under the same periods, rainfall is projected to increase in the months of October and December (40 and 10%), respectively, and decrease that varies from 25 to 40% (January to March). The Mafambisse station, however, presents a general decrease for both periods and RCPs, ranging from 20 to 40% in the first half of summer (October–December) and an increase of 10–20% for the second half of summer (January–March). Different projection of change is observed for Nhazonia and Pungwe Sul stations where the consistent decrease is observed with the range from 10 to 25% and 20 to 60% during all

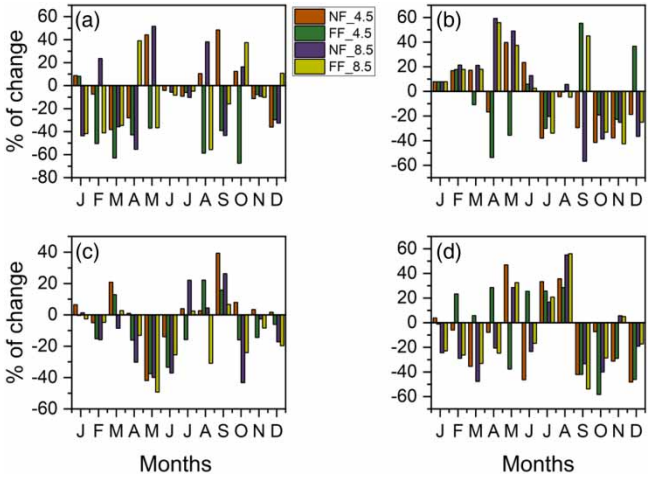

Figure 2 | Multi-model ensemble rainfall relative change for (a) Gorongosa Ponte, (b) Mafambisse, (c) Nhazonia, and (d) Pungwe Sul stations.

summer periods under RCP4.5 and RCP8.5 scenarios in all future periods. This rainfall distribution agrees with Shongwe *et al.* (2009) saying that a spatially coherent and significant reduction in mean rainfall is expected everywhere in southern Africa. Over Zimbabwe and central Mozambique, where the Pungwe River Basin is located, a reduction exceeding 20% is projected (Shongwe *et al.* 2009). Globally, the projected change in rainfall is expected to intensify the hydrological cycle leading to an increased risk and frequency of hydrological extremes such as floods (Gebrechorkos *et al.* 2023).

The results also show similarity with the one observed by Masimba *et al.* (2019) when assessing the baseline and downscaled projected climate variables in the Upper Manyame sub-catchment of Zimbabwe and concluded that the projected rainfall did not show a consistent increase or decrease in all the projected periods. However, the author verified that there will be a decline in the amount of rainfall during the onset of the rains that is October and an increase in the duration of the mid-season dry spell as shown by the decline in the amount of rainfall received in January. This indicates that the rainfall distributions do not show linear projections during the summer periods when most flood events occur and will impact negatively on the planning mitigation measures and call for the need of preparedness actions such as flood susceptibility mapping due to the shift in seasonal rainfall distribution that can lead to flash floods in the Pungwe River Basin (Ramayanti *et al.* 2022).

Projected change long-term monthly mean temperature

Projected change in maximum temperature

There is an increase in projected maximum temperature under RCP4.5 and RCP8.5 climate scenarios for all future periods and all the SAC stations (Figure 3). For both RCPs, the maximum temperature increasing trend varies from 0.1 to 1.9 °C for Gorongosa Ponte station in all months of the year and all periods. Under the same RCP, there is also a decreasing projection, the significant trend varies from 0.5 to 1.7 °C for the months of May, June, and December. Similarly, the Mafambisse and Nhazonia stations, resemble the same projections, where under RCP4.5 for 2050s and 2080s there is an increasing trend in maximum temperature that range from 0.1 to 2 °C in all the months. The maximum increase for the Mafambisse station is observed in the months of February, March, and October (2 °C) and for the Nhazonia station the maximum increase is observed in February, March and April. However, the RCP8.5 for Mafambisse and Nhazonia stations show a decrease of a maximum of 1.5 for the month of May and June and a maximum decrease of 1.8 °C for the month of November, respectively. The Pungwe Sul presents mixed projected behaviour, with the most expressive increasing trend observed for the months of summer (October–March) for both emissions scenarios and all future periods. The results agree with those presented by Masimba *et al.* (2019) although the magnitudes and range of increase are slightly different and also with the projections of IPCC (2021) for the Southern Africa region.

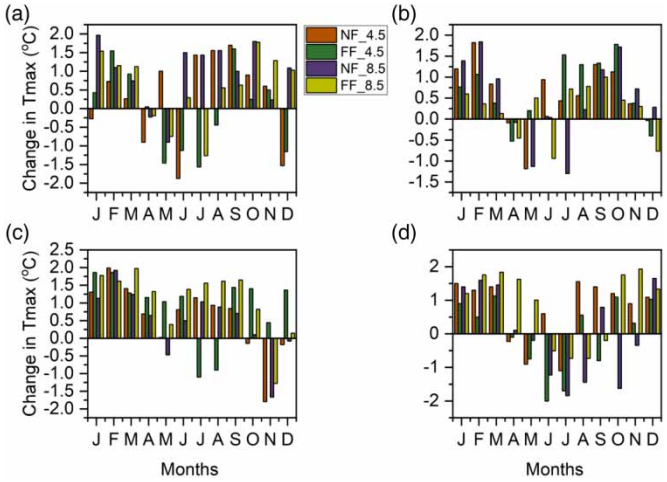

Figure 3 | Multi-model ensemble maximum temperature projected change for (a) Gorongosa Ponte, (b) Mafambisse, (c) Nhazonia, and (d) Pungwe Sul stations.

Projected change in minimum temperature

The minimum temperature as projected by the multi-model ensemble show, for RCP4.5 2050s and 2080s a generalised increase for Gorongosa Ponte, Mafambisse, and Pungwe Sul stations (Figure 4). There is an increasing minimum temperature projection for all months at the Gorongosa Ponte station, with the highest amount of change being verified in January, February, March, October, and December reaching 1.8 °C. However, it is also verified that the first summer months October and November will experience a decrease ranging from 1.5 to 1.7 °C. The decrease is also verified in the months of March and April under RCP8.5 of 2080s with a range of 1.2–1.5 °C. The Mafambisse station is also projected to experience higher minimum temperature as compared to the baseline period, reaching 2 °C under RCP8.5 in 2080s in the month of March. Under the RCP4.5 the other stations' experience increases that range from 0.5 to 1.5 °C in all the months of the year with an exception of February and November where a decrease (up to 1.5 °C) is expected (USAID 2020). The Nhazonia station shows a serious increase in temperature for the first semester of the year for both RCP4.5 and RCP8.5 for all future periods. This station also experience a decrease ranging from 0.5 to 2 °C in most of the months of the second semester of the year, for both RCPs and periods. An increasing trend is observed significantly in all months of the year, both RCPs and projected periods, reaching values up to 2 °C. The overall projection of minimum temperature for future periods shows an increasing trend (Adeola *et al.* 2022).

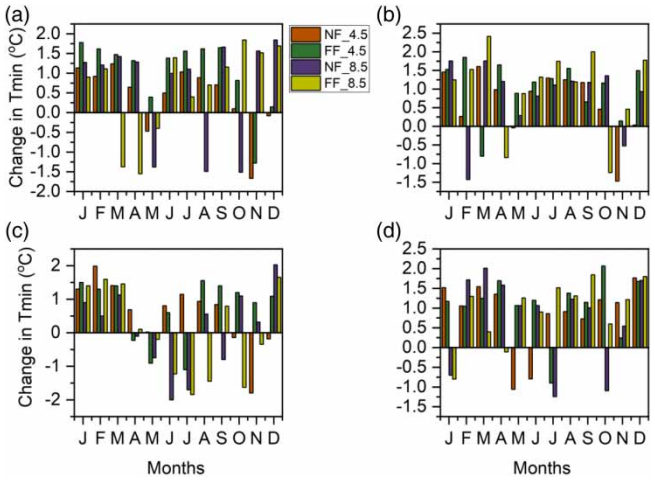

Figure 4 | Multi-model ensemble minimum temperature projected change for (a) Gorongosa Ponte, (b) Mafambisse, (c) Nhazonia, and (d) Pungwe Sul stations.

Calibration and validation of the HBV model

Model performance for the Gorongosa Ponte station

Table 4 shows the performance of the HBV model in simulating the streamflow during the calibration and validation processes. Figure 5 is the graphical representation of the coefficient of determination and the model efficiency indices.

Table 4 | HBV model performance during calibration (1999–2010) and validation (2011–2015) of runoff simulation

	Water balance [mm/year]		Goodness-of-fit				
Analyse	Q_{sim}	Q_{obs}	r^2	NSE	MD	EPF	σ
Calibration	958.58	962.63	0.89	0.88	4.04	0.91	3.67
Validation	1,168.39	1,086.97	0.82	0.83	7.07	0.84	6.41

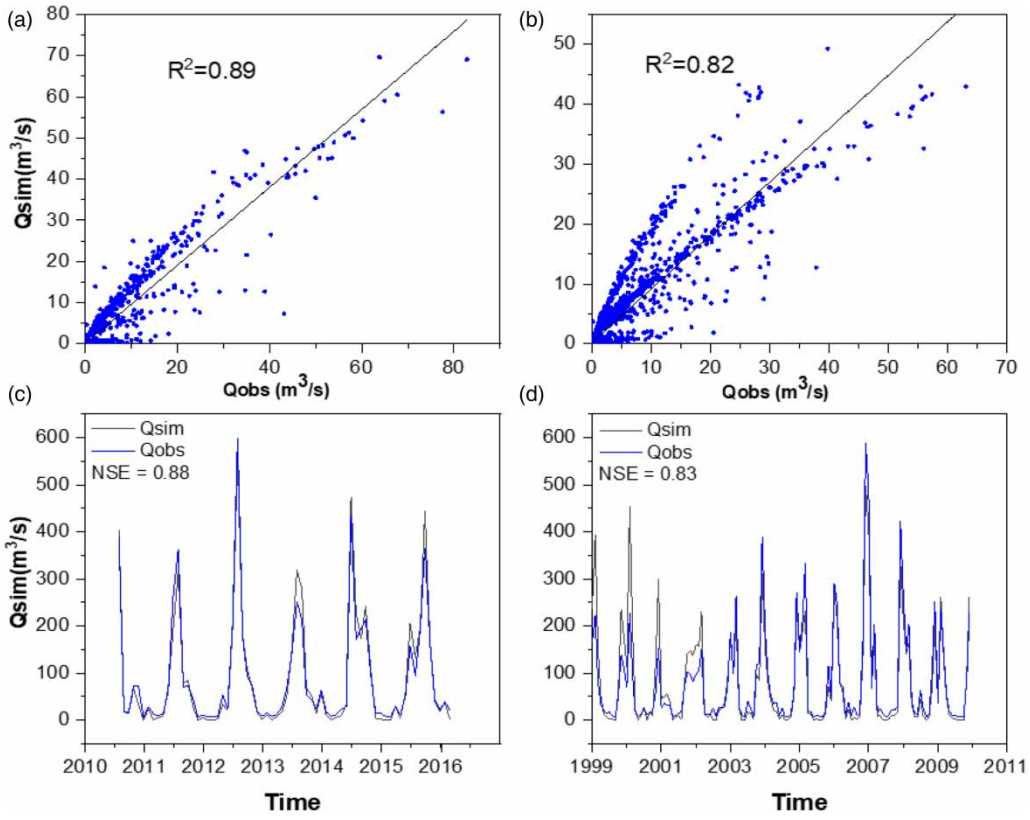

Figure 5 | Performance of the HBV model of runoff simulation and coefficient of determination: (a) calibration, (b) validation and model efficiency, (c) calibration, and (d) validation periods.

From Table 4, it can be depicted that the HBV model performed well in reproducing the peaks and baseflows during the calibration period (1999–2010), although there are some overestimations on peak flow during the simulation period. For the Ponte Gorongosa sub-catchment, the Nash–Sutcliffe efficiencies (NSE) obtained were 0.88 and 0.83, 0.89 and 0.82 for the coefficient of determination, 4.04 and 7.07 for mean difference, 0.91 and 0.84 for efficiency of the peak flow, and 3.67 and 6.41 for standard deviation during the calibration and validation period, respectively. These indices obtained suggest good model performance (Wubneh *et al.* 2023). The most sensitive parameters are the percentage of imperviousness and other parameters less sensitive but calibrated are: initial deficit, maximum deficit, and constant rate. Ramesh (2012) asserts that the proper characterisation of topography plays a vital role in runoff generation. Thus, the obtained objective function values indicate that the topographic-index distribution function for the catchment is adequate.

However, thou the performance of the model during calibration and validation periods is good, it must be noted the drawback caused by the lack of long series of data which led to the use of one single station with reliable runoff data for simulating the rest of the sub-basins, which limits the use of the model for future runoff simulation. The other drawback is that due to the scarcity of runoff data, it was not possible to calibrate and validate the model at the estuary of the basin and some of the flooded areas are located at downstream of the calibration and validation point. Hamutoko *et al.* (2022), in his study of the challenges associated with climate modelling in Africa concluded that the lack of seamless access to available data and the poor quality/missing data, often associated with the long-term measurement of climatic variables poses a great limitation.

Climate change impacts on streamflow

Projected changes in seasonal flows

Figure 6 shows the projected seasonal flows change for the Pungwe River Sub-basins. The multi-model ensemble projects an overall decrease in seasonal flows in all sub-basins and under both RCPs and future periods. The low flow in dry seasons mainly consists of subsurface flow and baseflow, which are generated from unsaturated and saturated soil zones (Wang *et al.* 2023). The October–November–December (OND) summer season, is the first part of the rain season in Mozambique, including the Pungwe River Basin area. The simulations of both RCP4.5 and 8.5 indicate for OND a decrease that ranges from 10 to 50% (50–100 m^3/s) for Nhazonia (a) and Muda (e) sub-basins. The other sub-basins present insignificant decreases as shown by the shapes of Figure 6. Different projection is shown for the second part of the summer season (January–February–March). All the sub-basins show a decreasing trend in a seasoned flow ranging from 20 to 60% (50–100 m^3/s). The potential impacts of climate change on streamflow have large uncertainty arising from a cascade of errors in the modelling chain (Clark *et al.* 2016). The simulated streamflow presented here can be affected by uncertainties in the RCP scenarios, the climate, and the hydrological model (Schumann 2021). While the aim of this paper is not to characterise the uncertainty in each component of the modelling chain, we highlight the potential contribution of each

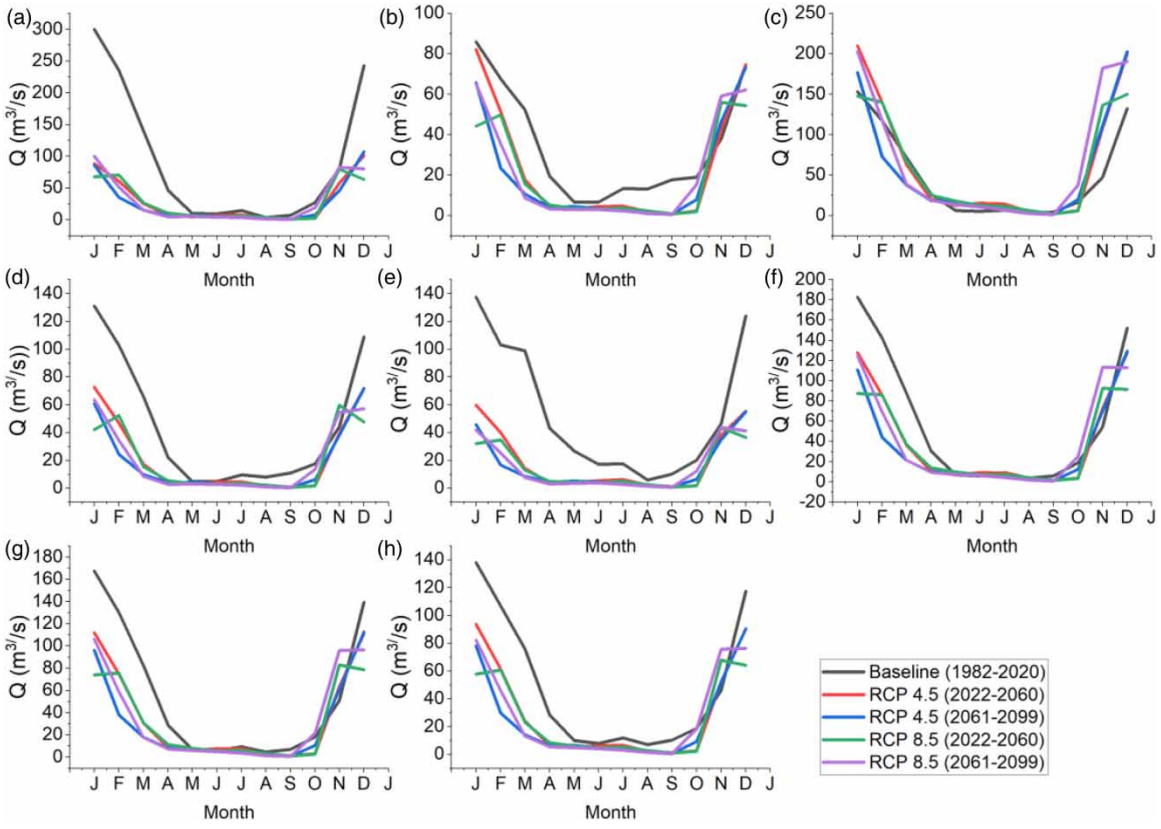

Figure 6 | Seasonal flows of baseline and the multi-model-ensemble projected changes: (a) Nhazonia, (b) PC Inferior, (c) Honde, (d) Vanduzi, (e) Muda, (f) PC Superior, (g) Urema, and (h) Bue Maria.

modelling component. Climate change will impact on availability and use of water resources in the Pungwe River Basin through the reduction of seasonal flow.

Projected changes extreme flow

Changes in future hydrological extremes flows were assessed by analysing changes in the high flow from baseline and the percent of change in 2050 and 2080s. Table 5 summarises changes in peak flow in different RCMs. An increase in extreme flow is projected under RCP4.5 for Honde, Vanduzi, and Bue Maria sub-basin ranging from 10 to 61% for 2050 and 2080s. Under the same emission scenario, there is an expected decrease from 5 to 30% in extreme flow for Nhazonia and PC Inferior sub-basin for both periods and for PC Inferior and Urema a range of 8–12% decrease in 2050s. For RCP8.5, an increase in extreme events is projected for Honde, PC Superior, Vanduzi, Muda, Urema, and Bue Maria sub-basins. The range of increase varies from 11 to 104% for all future periods. The increase in extremely high flows, which is associated with floods, will impact negatively in many parts of Central Mozambique.

Table 5 | Changes in extreme flow in the Pungwe River Basin

Sub-basins	Baseline (1982–2020)	RCP4.5 2050s	RCP4.5 2080s	Baseline (1982–2020)	RCP8.5 2050s	RCP8.5 2080s	Variables
Nhazonia	306.5	163.3	212.8	306.5	274.8	207.7	Peak runoff (m^3/s)
		−46.7	−30.6		−10.4	−32.2	Change (%)
		11.4	17.1		15.5	16.6	Min. runoff (m^3/s)
		38.6	46		52.8	42.3	Standard Deviation
PC Inferior	117.5	86.1	111.3	117.5	114.8	65.1	Peak runoff (m^3/s)
		−26.8	−5.3		−2.3	−44.6	Change (%)
		8.2	11.2		13.4	8	Min. runoff (m^3/s)
		19.9	24.6		22.1	15	Standard Deviation
Honde	137.2	181.2	202.1	137.2	279.9	271.6	Peak runoff (m^3/s)
		32.1	47.4		104.1	98	Change (%)
		21.4	24.6		28.4	36.2	Min. runoff (m^3/s)
		37.2	44.3		55.2	47	Standard Deviation
Vanduzi	96.3	106.6	155.2	96.3	173.8	94.6	Peak runoff (m^3/s)
		10.7	61.2		80.5	−1.7	Change (%)
		5.8	9.2		8.9	10.1	Min. runoff (m^3/s)
		22.4	32.1		31.1	19.9	Standard Deviation
Muda	139.2	75.3	82	139.2	106.6	69.9	Peak runoff (m^3/s)
		−45.9	−41		−23.4	−49.8	Change (%)
		8.7	10.5		14.3	9.5	Min. runoff (m^3/s)
		17.9	17.7		19.9	16.8	Standard Deviation
PC Superior	156	136.5	168	156	228.7	182.1	Peak runoff (m^3/s)
		−12.5	7.7		46.6	16.7	Change (%)
		13.6	16.5		19.8	21.4	Min. runoff (m^3/s)
		29.9	34.3		41.2	32.3	Standard Deviation
Urema	135.3	124.2	160	135.3	209.4	151.3	Peak runoff (m^3/s)
		−8.2	18.3		54.8	11.8	Change (%)
		11.8	14.4		18.5	18.1	Min. runoff (m^3/s)
		27.1	32.6		37	27.7	Standard Deviation
Bue Maria	81.5	102.1	128	81.5	160.5	101.1	Peak runoff (m^3/s)
		25.3	57		96.9	24	Change (%)
		9.5	12		14.9	13.7	Min. runoff (m^3/s)
		22.6	27.3		27.8	20	Standard Deviation

Flood inundation extent simulations in HEC-RAS

Projected changes in flooded areas, validation of flood map and impact assessment

Using observed peak discharge values statistically predicted from the Gumbel distribution and RCM ensemble peak discharge values, steady flow simulations were performed in HEC-RAS. The simulations on the Gumbel

distribution were based on the 50-, 100-, and 1,000-year return periods. Future flood simulations were regarding RCP4.5 and RCP8.5 scenarios, 2050s and 2080s future periods on daily timestep. After running various simulations in HEC-RAS, the data were exported to QGIS, where flood-inundated areas were determined. In the multi-model ensemble, the 100-year return period continues to be one with maximum flood extent with values of 5,041 and 5,657 km^2 for 2050s and 2080s under RCP8.5. To assess the HEC-RAS model reliability in simulating floods of a given magnitude, a flood map from 19 March 2019 during cyclone Idai captured by Sentinel 1 was used to validate the map of the simulated flood of the same period, the overlay method applied (Khattak *et al.* 2016). Therefore, a comparison of both maps (observed and simulated) was made. Figure 7 shows the extent of inundation shown by Sentinel 1 image and by the model flood matched closely considering that only main rivers were flood modelled, with small deviations. These deviations could be attributed to the way the water surface is generated by the GIS software (Afzal *et al.* 2022). Several approaches are used to simulate and map floods, however, due to the highly complex nature of meteorological and hydrological processes, it is not possible to forecast extreme precipitation events that lead to catastrophic floods (Khattak *et al.* 2016). Therefore, the approach here applied can be an aid in developing countries such as Mozambique where humans are particularly vulnerable to flooding because of high population density, absence of adequate flood control measures, and lack of zoning regulations and emergency preparedness systems.

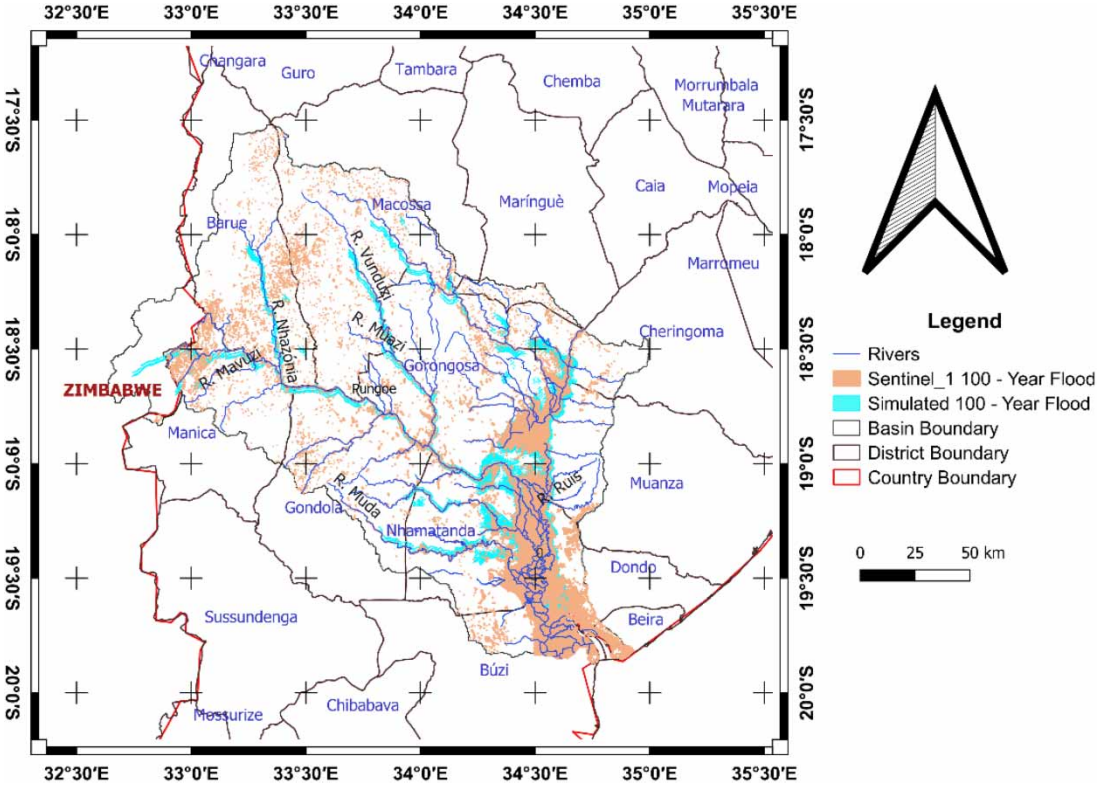

Figure 7 | Comparison between simulated and actual (Sentinel 1 image taken on 19 March 2019 during Cyclone Idai) 100-year flood extents.

As the projected situation illustrates, it is expected that future flood inundation extension be greater if compared to the actual period, this will cause damage to infrastructure as compared to the damage that took place during the cyclone Idai-induced flood (Ramayanti *et al.* 2022). It is projected that there will be great negative impacts on schools, hospitals, houses, and livestock mainly of riverine people. Water and infrastructure planners need to look for strategies for mitigation of the effects of climate change by looking at future inundated areas as indicated by the map in Figure 7, this includes the construction of flood structures (Afzal *et al.* 2022), such as dams and impoundments.

CONCLUSIONS

This study has demonstrated the integrated application of a series of tools with the objective of mapping the future extent of flood under climate change using the Pungwe River Basin as an example. While the assessment of the climate change impact is not demonstrated in full, the results demonstrate, however, the significant vulnerability that the basin is facing. The analysis of the historical and projected hydrological and meteorological series is important and even more relevant when considering the localised effects of global climate change. Therefore, to detect climate change and analyse the climatic parameters. The main conclusions of our work are:

- The multi-model ensemble performed better in simulating the projected climate variables of the Pungwe River Basin in mimicking rainfall. There is no consistency in the projected signal of rainfall and temperature compared to the baseline. In general, there is an increasing projected change in temperature time series up to 15% and an inversely decreasing projection of change in rainfall time series in the stations located in the Pungwe River Basin. Results on projected rainfall, temperature and streamflow accretion would help to develop effective adaptation measures for reducing the impacts of climate change and to work out long-term water resource management plans in the river basin.
- The HBV model performed well in reproducing the extreme and seasonal flow during the calibration (1999–2010) and validation (2011–2015) periods with the Nash–Sutcliffe efficiencies (NSE) of 88 and 83%, respectively. In peak flow change analysis, it was observed that in the future is projected an overall increase in peak flow is up to 100%, leading to the occurrence of more frequent and intense flood events. There is a clear indication that climate change will impact in river basin flow, reducing the seasonal flow and increasing the extreme flows. This will reduce water availability and also influence the occurrence of flood events.
- In flood extent, an increase of the inundation area is projected with the return period of 100 years for 2080s, giving the overall maximum expected flood for the Basin under RCP8.5 extension of 5,041 km^2. The cyclone Idai-induced flood map from Sentinel 1 matched perfectly with simulated flood mapping, making the approach useful to validate map future flood events. While these results are obtained, there is a need of need for the integration of other factors that trigger floods such as land-use, and population density (urbanisation). Moreover, these results may change if new developments are seen in the Basin such as the construction of flood structures such as dams and impoundments. The results suggest that the population that live in river basins that might inevitably be affected by increased flood events during climate change. The last conclusion is associated with the uncertainty bound to climate change models. It is, however, well documented in the literature, while the aim of this paper is not to discuss this matter, it must be noticed that there is a chance that these results may be affected by this uncertainty and decision makes the need to consider when making plans with outputs from this research and the idea was giving a guideline for analysis of climate change impacts in extremes, mainly floods.

RECOMMENDATIONS

There is a need of development of more research analysing climate change, landuse, and urbanisation in the Pungwe River Basin. Modelling of extreme events requires the existence of long-term hydroclimatic quality data. Therefore, the ARA-CENTRO needs to improve the strategy of data manipulation from the collection methods, processing, and storage to avoid over- and under-estimating water resources and their flows and aid in proper data-driven solutions.

DATA AVAILABILITY STATEMENT

All relevant data are included in the paper or its Supplementary Information.

CONFLICT OF INTEREST

The authors declare there is no conflict.

REFERENCES

Adeola, A. M., Kruger, A., Makgoale, T. E. & Botai, J. O. 2022 Observed trends and projections of temperature and precipitation in the Olifants River Catchment in South Africa. *PLoS One* **17**, 1–21. https://doi.org/10.1371/journal.pone.0271974.

Afzal, M. A., Ali, S., Nazeer, A., Khan, M. I., Waqas, M. M., Aslam, R. A., Cheema, M. J. M., Nadeem, M., Saddique, N. & Muzammil, M. 2022 Flood inundation modeling by integrating HEC–RAS and satellite imagery: a case study of the Indus River Basin. *Water* **14**, 2984.

Bergström, S. 1976 The HBV model – its structure and applications. *Swedish Meteorol. Hydrol. Institute. Norrköping* **4**, 1–33.

Brassel, K. E. & Reif, D. 1979 A procedure to generate Thiessen polygons. *Geogr. Anal.* **11**, 289–303.

Brunner, G. 2008 HEC-RAS_4.0_Reference_Manual.pdf.

Chakraborty, S. & Mukhopadhyay, S. 2019 Assessing flood risk using analytical hierarchy process (AHP) and geographical information system (GIS): application in Coochbehar district of West Bengal, India. *Nat. Hazards* **99**, 247–274.

Chen, Y.-J., Lin, H.-J., Liou, J.-J., Cheng, C.-T. & Chen, Y.-M. 2022 Assessment of flood risk map under climate change RCP8. 5 scenarios in Taiwan. *Water* **14**, 207.

Chipere, T., Gumindoga, W., Rwasoka, D. & Mhizha, A. 2020 Future Flood Inundations under Climate Change Scenarios : A case of Middle Zambezi Basin in Zimbabwe Future Flood Inundations under Climate Change Scenarios.

Clark, M. P., Wilby, R. L., Gutmann, E. D., Vano, J. A., Gangopadhyay, S., Wood, A. W., Fowler, H. J., Prudhomme, C., Arnold, J. R. & Brekke, L. D. 2016 Characterizing uncertainty of the hydrologic impacts of climate change. *Curr. Clim. Change Rep.* **2**, 55–64.

Demissie, T. A. & Sime, C. H. 2021 Assessment of the performance of CORDEX regional climate models in simulating rainfall and air temperature over southwest Ethiopia. *Heliyon* **7**, e07791. https://doi.org/10.1016/j.heliyon.2021.e07791.

Desalegn, H. & Mulu, A. 2021 Mapping flood inundation areas using GIS and HEC-RAS model at Fetam River, Upper Abbay Basin, Ethiopia. *Sci. Afr.* **12**. https://doi.org/10.1016/j.sciaf.2021.e00834.

Dibaba, W. T., Miegel, K. & Demissie, T. A. 2019 Evaluation of the CORDEX regional climate models performance in simulating climate conditions of two catchments in Upper Blue Nile Basin. *Dyn. Atmos. Oceans* **87**, 101104.

Di Baldassarre, G., Martinez, F., Kalantari, Z. & Viglione, A. 2017 Drought and flood in the Anthropocene: feedback mechanisms in reservoir operation. *Earth Syst. Dyn.* **8**, 225–233.

Gaisie, E. & Brandful, P. 2023 Planning for context-based climate adaptation : flood management inquiry in Accra. *Environ. Sci. Policy* **141**, 97–108. https://doi.org/10.1016/j.envsci.2023.01.002.

Gebrechorkos, S. H., Taye, M. T., Birhanu, B., Solomon, D. & Demissie, T. 2023 Future changes in climate and hydroclimate extremes in East Africa. *Earth's Future* **11**(2), https://doi.org/10.1029/d2022EFd003011.

Government of Mozambique 2019 *Mozambique Cyclone Idai: Post Disaster Needs Assessment 243*.

Grežo, H., Močko, M., Izsoff, M., Vrbičanová, G., Petrovič, F., Straňák, J., Muchova, Z., Slamova, M., Olah, B. & Machar, I. 2020 Flood risk assessment for the long-term strategic planning considering the placement of industrial parks in Slovakia. *Sustainability* **12**, 4144.

Gumindoga, W., Rwasoka, D. T., Nhapi, I. & Dube, T. 2016 Ungauged runoff simulation in Upper Manyame Catchment, Zimbabwe : application of the HEC-HMS model. *Phys. Chem. Earth* 1–12. https://doi.org/10.1016/j.pce.2016.05.002.

Guo, J., Luan, Y., Li, Z., Liu, X., Li, C. & Chang, X. 2021 Mozambique flood (2019) caused by tropical cyclone idai monitored from sentinel-1 and sentinel-2 images. *IEEE J. Sel. Top. Appl. Earth Obs. Remote Sens.* **14**, 8761–8772.

Habib, E., Haile, A. T., Sazib, N., Zhang, Y. & Rientjes, T. 2014 Effect of bias correction of satellite-rainfall estimates on runoff simulations at the source of the Upper Blue Nile. *Remote Sens.* **6**, 6688–6708. https://doi.org/10.3390/rs6076688.

Hamutoko, J., Oluwagbemi, O., Fotso-Nguemo, T. C. & Lokonon, B. O. K. 2022 Towards resolving challenges associated with climate change modelling in Africa. https://doi.org/10.3390/app12147107.

Hegdahl, T. J., Engeland, K., Steinsland, I. & Singleton, A. 2023 Pre-and postprocessing flood forecasts using Bayesian model averaging. *Hydrol. Res.* **54**, 116–135.

IPCC 2014 *Climate Change 2014: Synthesis Report. Contribution of Working Groups I, II and III to the Fifth Assessment Report of the Intergovernmental Panel on Climate Change*. Geneva, Switzerland.

IPCC 2021 *Climate Change 2021: The Physical Science Basis. Contribution of Working Group I to the Sixth Assessment Report of the Intergovernmental Panel on Climate Change*. Cambridge Univ. Press.

Januário, T. E., José, A., Filho, P. & Salviano, M. F. 2022 Hydrometeorological modeling of Limpopo River Basin in Mozambique with TOPMODEL and remote sensing. *Open J. Mod. Hydrol.* **12**, 55–73. https://doi.org/10.4236/ojmh.2022.122004.

Kalantari, Z., Ferreira, C. S. S., Keesstra, S. & Destouni, G. 2018 Nature-based solutions for flood-drought risk mitigation in vulnerable urbanizing parts of East-Africa. *Curr. Opin. Environ. Sci. Health* **5**, 73–78. https://doi.org/10.1016/j.coesh.2018.06.003.

Khattak, M. S., Anwar, F., Saeed, T. U., Sharif, M., Sheraz, K. & Ahmed, A. 2016 Floodplain mapping using HEC-RAS and ArcGIS: a case study of Kabul River. *Arab. J. Sci. Eng.* **41**, 1375–1390.

Korah, P. I. & Cobbinah, P. B. 2019 Institutional Responses to Climate Change Adaptation: Flood Management at the Metropolitan Level in Accra, Ghana. In: Cobbinah, P.B., Addaney, M. (eds) The Geography of Climate Change Adaptation in Urban Africa. Palgrave Macmillan, Cham. https://doi.org/10.1007/978-3-030-04873-0_16.

Lawin, A. E., Hounguè, N. R., Biaou, C. A. & Badou, D. F. 2019 Statistical analysis of recent and future rainfall and temperature variability in the Mono River Watershed. *Climate*. https://doi.org/10.3390/cli7010008.

Liu, W.-C., Hsieh, T.-H. & Liu, H.-M. 2021 Flood risk assessment in urban areas of southern Taiwan. *Sustainability* **13**, 3180.

Maathuis, B. H. P. & Wang, L. 2006 Digital elevation model based hydro - processing digital elevation model based hydro-processing. *Geocarto Int.* **21**(1), 21–26. https://doi.org/http://dx.doi.org/10.1080/10106040608542370 PLEASE.

Masimba, O., Gumindoga, W., Mhizha, A. & Rwasoka, D. T. 2019 An assessment of baseline and downscaled projected climate variables in the Upper Manyame sub-catchment of Zimbabwe. *Phys. Chem. Earth* 1–14. https://doi.org/10.1016/j.pce.2019.07.001.

Nharo, T., Makurira, H. & Gumindoga, W. 2019 Mapping floods in the middle Zambezi Basin using earth observation and hydrological modeling techniques. *Phys. Chem. Earth* **114**, 1–9. https://doi.org/10.1016/j.pce.2019.06.002.

Nyabeze, W. R. 2021 *Determining Precipitation Patterns for the Buzi, Pungwe and Save River Catchments with the Framework for Using Open Source Software to Analyze Large Gridded Data (FOSS-LGD)*.

Poméon, T., Jackisch, D. & Diekkrüger, B. 2017 Evaluating the performance of remotely sensed and reanalysed precipitation data over West Africa using HBV light. *J. Hydrol.* **547**, 222–235.

Rahmati, O., Zeinivand, H. & Besharat, M. 2016 Flood hazard zoning in Yasooj region, Iran, using GIS and multi-criteria decision analysis. *Geomatics, Nat. Hazards Risk* **7**, 1000–1017.

Ramayanti, S., Nur, A. S., Syifa, M., Panahi, M., Achmad, A. R., Park, S. & Lee, C.-W. 2022 Performance comparison of two deep learning models for flood susceptibility map in Beira area, Mozambique. *Egypt. J. Remote Sens. Space. Sci.* **25**, 1025–1035.

Ramesh, A. 2012 *Response of Flood Events to Land Use and Climate Change: Analyzed by Hydrological and Statistical Modeling in Barcelonnette, France*. Springer Science & Business Media.

Schumann, G. J.-P. 2021 *Earth Observation for Flood Applcations – Progress and Perspectives*. London. https://doi.org/10.1007/978-94-007-5527-7.

Schumann, G. J. P., Brakenridge, G. R., Kettner, A. J., Kashif, R. & Niebuhr, E. 2018 Assisting flood disaster response with earth observation data and products: a critical assessment. *Remote Sens.* **10**, 1–19. https://doi.org/10.3390/rs10081230.

Shongwe, M. E., Van Oldenborgh, G. J., Van Den Hurk, B., De Boer, B., Coelho, C. A. S. & Van Aalst, M. K. 2009 Projected changes in mean and extreme precipitation in Africa under global warming. Part I: Southern Africa. *J. Clim.* **22**, 3819–3837.

SWECO and Associates 2004 *Development of the Pungwe River Basin Joint Integrated Water Resources Management Strategy. Final Report*. Swedish Int. Dev. Coop. Agency.

Uamusse, M. M., Ndalila, P., JúlioTsamba, A. & Carvalho, F. d. O. 2015 Monthly stream flow predition in Pungwe River for small hydropower plant using wavelet method. *Int. J. Energy Power Eng.* **4**, 280. https://doi.org/10.11648/j.ijepe.20150405.17.

UNDP 2019 Mozambique Cyclone Idai Post-Disaster Needs Assessment (PDNA) DNA | United Nations Development Programme [WWW Documen]. UNDP.

USAID 2020 Climate Change Information Fact Sheet, Ethiopia 2030, 1–7.

Van Tiel, M., Stahl, K., Freudiger, D. & Seibert, J. 2020 Glacio-hydrological model calibration and evaluation. *Wiley Interdiscip. Rev. Water* **7**, e1483.

Wang, Y., Wang, Y., Wang, Y., Li, C., Ju, Q., Jin, J., Deng, X., Sun, G. & Bao, Z. 2023 Applicability of the HBV model to a human-influenced catchment in northern China. *Hydrol. Res.* **54**(2).

Williamson, C., Mccordic, C. & Doberstein, B. 2023 The compounding impacts of Cyclone Idai and their implications for urban inequality. *Int. J. Disaster Risk Reduct.* **86**, 103526. https://doi.org/10.1016/j.ijdrr.2023.103526.

Worku, G., Teferi, E., Bantider, A., Dile, Y. T. & Taye, M. T. 2018 Evaluation of regional climate models performance in simulating rainfall climatology of Jemma sub-basin, Upper Blue Nile Basin, Ethiopia. *Dyn. Atmos. Oceans* **83**, 53–63.

Wubneh, M. A., Worku, T. A. & Chekol, B. Z. 2023 Climate change impact on water resources availability in the kiltie watershed, Lake Tana sub-basin, Ethiopia. *Heliyon* **9**, e13941. https://doi.org/10.1016/j.heliyon.2023.e13941.

Yue, S., Che, Y., Chang, H., Tsung, C., Shiang, H. & Wu, J. 2022 Variation of uncertainty of drainage density in flood hazard mapping assessment with coupled 1D – 2D hydrodynamics model. *Nat. Hazards* **111**, 2297–2315. https://doi.org/10.1007/s11069-021-05138-1.

Zare, M. & Schumann, G. J. 2021 Emerging techniques in machine learning for processing satellite images of floods. In: *Earth Observation for Flood Applications*. Elsevier Ltd, pp. 321–336. https://doi.org/10.1016/B978-0-12-819412-6/00015-8.

First received 15 December 2021; accepted in revised form 6 April 2023. Available online 21 April 2023